

SYSTEMS, SCIENCE AND SOFTWARE

SSS-R-74-2029

EXPLOR
(EXAMINATION OF POLLUTION LEVELS OF ROADWAYS)
VOLUME I THEORY AND VALIDATION
FINAL TECHNICAL REPORT

J. W. Kirsch
B. F. Mason

Sponsored by:
California Air Resources Board
Contract Number: ARB-659

15 January 1974

LIBRARY
AIR RESOURCES BOARD
P. O. BOX 2815
SACRAMENTO, CA 95812

ABSTRACT

EXPLOR, a conservation of mass mathematical model with a second order advection-diffusion scheme, is used to calculate off-roadway, ground level carbon monoxide concentrations. EXPLOR has been validated to within the experimental error of the supplied traffic data.

This report was submitted in fulfillment of ARB-659 under the sponsorship of the California Air Resources Board. Work was completed as of January 1974.

TABLE OF CONTENTS

	<u>Page</u>
SECTION 1 — CONCLUSIONS	I-1
SECTION 2 — RECOMMENDATIONS	I-2
SECTION 3 — INTRODUCTION	I-3
3.1 Background	I-3
3.2 Purpose	I-3
3.3 Project Phases	I-3
3.4 Theory	I-4
SECTION 4 — THE EXPLOR CODE	I-15
4.1 Validation	I-15
4.1.1 Data	I-15
4.1.2 Methodology	I-18
4.1.3 Basic Results	I-25
4.1.4 Estimate of Experimental Error	I-25
4.1.5 Sources of Error	I-32
4.2 Discussion	I-36
REFERENCES	I-38
PUBLICATIONS	I-40
GLOSSARY OF SYMBOLS	I-41
GLOSSARY OF SYMBOLS FOR APPENDIX A ONLY	I-43
APPENDIX A — THREE-DIMENSIONAL EXPLOR	I-44
APPENDIX B — SAMPLE 3D CALCULATION	I-49

LIST OF TABLES

<u>Table</u>		<u>Page</u>
1	Variation of P	I-7
2	Variations in σ_{ϵ}	I-9
3	Turbulence Scale Lengths (l)	I-9
4	Input Data "At-grade" Section	I-22
5	Input Data - "Fill" Section	I-23
6	Input Data - Cut I Sections	I-23
7	Input Data - Cut II Section	I-24
8	Basic EXPLOR Validation Results	I-25
9	EXPLOR Validation Results - Near Roadway Versus Far Roadway	I-33
10	EXPLOR Validation Results for Different Cross-Wind Angles	I-34
11	EXPLOR Validation Results - Rush Hour Versus Normal Traffic	I-35
12	EXPLOR Validation Results - Atmospheric Stability	I-36

LIST OF FIGURES, CONTINUED

<u>Figure</u>		<u>Page</u>
B.3	Contour plot for CO in the X-Z plane at the third Y cell	I-53
B.4	Contour plot for CO in the Y-Z plane at the third X cell	I-54

ACKNOWLEDGEMENTS

The authors would like to thank Messrs. Samuels and Ranzieri and the late Mr. Hutchinson of the ARB for their aid in the conduct of this program. They also wish to express their appreciation to Messrs. T. Smith and S. Howard (Meteorology Research, Inc.) for their participation in this study.

1. CONCLUSIONS

The EXPLOR code, a mathematical model to predict off roadway, ground level CO concentrations resulting from freeways, is currently available for production use. EXPLOR has been validated by comparing predicted concentrations to measured data taken at four California locations. These included at-grade, cut and fill sections. The calculated values had a mean error of -0.34 ppm and a standard deviation of 1.09 ppm. This is within the estimated error band due to inaccuracies in the experimental data.

2. RECOMMENDATIONS

The EXPLOR code has been designed to be used under a wide variety of geometrical and meteorological conditions. For this reason, no specific limitations are noted, although the user should be aware of certain facts:

- 1) EXPLOR has been validated for at-grade, cut, and fill geometries. Bridges and viaducts (in which there is air flow under the roadway) may also be used, but for these latter cases no validating data was available.
- 2) Although there is no reason to doubt EXPLOR calculations at distances up to one mile from the roadway, validating data was available only to a maximum distance of 600 feet.
- 3) Major changes in concentration can occur with variation of the stability class. For this reason, the user must be very careful in determining the correct stability class.

3. INTRODUCTION

3.1 BACKGROUND

Prior to the present development study, several computer codes existed which calculated carbon monoxide (CO) concentrations arising from freeway sources. These codes depended on the Gaussian approximation and dealt primarily with at-grade road geometries. The lack of physics written into these codes precluded their accurate extension to more complex geometries and consideration of wind flows around terrain features.

3.2 PURPOSE

The purpose of the present work was the formulation and validation of a mathematical model which would be able to predict CO concentrations for more general highway cases. The model was named EXPLOR (EXamination of Pollution Levels Of Roadways). By virtue of containing much more physics, EXPLOR would also be more accurate than the earlier codes. To be included were the effects of advection and diffusion on the pollutant concentration, as well as the effects of terrain features on the wind field.

3.3 PROJECT PHASES

The construction of the code was accomplished by

first developing and coding a basic advection-diffusion scheme for the transport of gaseous material. The next step was to include complex wind fields, as determined by the terrain, and to make the diffusion model more realistic. Both of the latter tasks involved the aid of a subcontractor (Meteorology Research, Inc.) which provided data for accurate understanding and modeling of the meteorological phenomena in question. Validation studies were then conducted on the two dimensional version of the code (three dimensional data never did become available).

3.4 THEORY

The mathematical basis of EXPLOR is the numerical, finite-difference solution of the advection-diffusion equation describing the conservation of mass of the pollutant, i.e.,

$$\frac{\partial c}{\partial t} + \vec{u} \cdot \vec{\nabla} c = \vec{\nabla} \cdot (\underline{k} \cdot \vec{\nabla} c) + S \quad (1)$$

where

c = pollutant concentration

\vec{u} = mean wind velocity

\underline{k} = turbulent diffusivity tensor

S = emission source strength

In this framework, the pollutant is advected by the mean fluid motion and dispersed by the turbulent mixing processes, as modeled by the diffusivity terms, $\vec{\nabla} \cdot (\underline{k} \cdot \vec{\nabla} c)$, in Eq. (1). The emission of pollutants is modeled by the inclusion of the source term, S . Basically, pollutants are introduced at source cells (located at the roadway), and at each time step, Δt , a metered amount of pollutant is added to the source.

The pollutant is advected and diffused by the winds until steady state is reached.

Both advection and diffusion are treated in the code by using a Crowley ⁽¹⁾ second-order scheme. In EXPLOR, any quantity, Ω , to be advected in the x-direction (for example) is given by

$$\Omega_i^{n+1} = \Omega_i^n + \frac{\Delta t}{\Delta x_i} (F_i - F_{i+1}) \quad (2)$$

where Δt is the time step, the i subscript denotes the zone number, and F is a flux term which is a function of the form

$$F_i = [(u\Omega)_{(i+1)} - (u\Omega)_i] \quad , \quad (3)$$

u being the x-velocity component. Diffusion is treated by replacing the mean velocity in (3) with a diffusion transport velocity (see Appendix A).

It is evident that wind-field ($\vec{u}(x,y)$), diffusivity formulation ($\underline{k}(\vec{u},x,y)$), and source models (S) are required to numerically integrate Eq. (1). The wind-field calculation should include both tangential and vertical components of the velocity. Since highways are generally located in the near surface atmospheric boundary layer ($h < 100$ m), the vertical gradient of the tangential velocity must be taken into account, as well as the variations in eddy diffusivity in the near surface region. These effects have been incorporated into the EXPLOR model.

The wind field in EXPLOR calculations is computed on the basis of an ad hoc prescription suggested by Lantz, et al. ⁽²⁾ to take into account the wind shear that exists in the near surface atmospheric boundary layer. The usual definition of the velocity potential, i.e.,

$$\vec{u} = \vec{\nabla}\phi \quad (4)$$

is modified by a potential coefficient tensor, $\underline{\lambda}$,

$$\vec{u} = \underline{\lambda}\vec{\nabla}\phi \quad (5)$$

when $\underline{\lambda}$ can be prescribed to fit the wind conditions to be simulated. In EXPLOR, the current prescription for λ_{ij} is

$$\lambda_{ij} = 0 \quad , \quad i \neq j \quad (6)$$

$$\lambda_{11} = (z/z_0)^p \quad (7)$$

$$\lambda_{22} = \lambda_{33} = 1 \quad (\text{except at boundaries where} \quad (8)$$

$$\lambda_{22} = 0)$$

where

z = height above the ground

z_0 = reference height

p = stability class parameter

The values for p vary with stability conditions. EXPLOR incorporates those reported by DeMarrais,^[3] and values are given in the following table:

TABLE 1
Variation of P

Pasquill Class	P
A	0.15
B	0.17
C	0.20
D	0.26
E	0.39
F	0.48
G	0.54

Note that with this prescription for λ (Eqs. (6) and (7)), the linear field, $\phi \propto x$, will automatically reduce to a sheared profile consistent with the specified stability class.

In general, the prediction of the turbulent diffusivity at an arbitrary point in the wind field is based on the relationship that

$$k \propto u' \ell \quad (9)$$

where

k = diffusivity, ft²/sec

u' = turbulent fluctuation velocity at which turbulent energy is maximized, ft/sec

ℓ = turbulence length scale, ft

[Dimensions are given in the British Engineering

Systems to match EXPLOR units.]

The EXPLOR model incorporates a model suggested by Smith and Howard, [4]

$$k_{22} = 0.45 u \sigma_{\epsilon} \ell \quad (10)$$

where

u = local wind speed, ft/sec

σ_{ϵ} = mean wind vane fluctuation (radians/sec)

Both σ_{ϵ} and ℓ are functions of the Pasquill stability class and height above the ground. The values have been taken from Smith and Niemann, [5] and Taylor, et al., [6] and are presented in Tables 2 and 3. The diffusion length scale, k/u , varies from 0.105 ft to 40.2 ft as conditions vary from near surface, highly stable winds to 328 ft heights and unstable air flows.

If desired, a diffusivity field can be patched into the EXPLOR grid and a special option has been included that forces the diffusivity to a constant value throughout the grid. At solid boundaries the diffusivity is set equal to zero in the direction normal to the surface.

The wind field is calculated by solving the continuity equation, i.e.,

$$\vec{\nabla} \cdot \vec{u} = 0 = \vec{\nabla} \cdot \underline{\lambda} \vec{\nabla} \phi \quad (11)$$

in a finite difference grid which includes block models of major topographical features and structures that present impermeable slip boundaries to the flow.

In practice, ϕ is obtained by assuming an initial value and then using the line successive over-relaxation

TABLE 2

Variations in σ_ϵ (Smith and Niemann, 1969)

Stability Class	σ_ϵ (32.8 feet)	σ_ϵ (98.5 and 328 ft)
A	0.200 radians	0.262
B	0.185	0.237
C	0.157	0.184
D	0.117	0.119
E	0.061	0.056
F	0.028	0.023
G	0.012	0.009

TABLE 3

Turbulence Scale Lengths (l) (Taylor, Warner and Bacon, 1970)

Height	Stability Class						
	A	B	C	D	E	F	G
32.81 ft	59.06	49.21	39.37	32.81	26.25	22.97	19.69
65.62	98.34	82.02	68.90	59.06	52.49	45.93	39.37
98.43	134.51	111.55	95.14	82.02	72.18	65.62	55.77
164.04	203.41	170.60	144.36	127.95	114.83	101.71	88.58
246.06	275.59	232.94	196.85	170.60	157.48	141.08	121.39
328.08	344.49	278.87	242.78	209.97	196.85	177.17	150.92

technique, where

$$\phi_{ij}^{n+1} = \alpha \phi_{ij}^{n+\frac{1}{2}} + (1-\alpha) \phi_{ij}^n \quad (12)$$

where

$$\alpha > 1$$

$$n = \text{iteration number}$$

Experience has shown that the solution converges ($\phi^{n+1} \approx \phi^n$) after twenty iterations.

The horizontal wind (which is boundary centered) is calculated from

$$u = \sum \lambda_{ij} \cdot \frac{(\phi_{ij} - \phi_{i-1,j})}{\Delta x_{i-1}^a} \quad (13)$$

where Δx^a is the distance in the x-direction from cell center to cell center and ϕ is cell centered.

The horizontal wind field is then modified by the input data to provide a least-squares fit between the calculated wind field (u^c) and the given wind data (u^m) by taking

$$\delta = \frac{\sum_{i=1}^n u_i^c u_i^m}{\sum_{i=1}^n u_i^c u_i^c} \quad (14)$$

when n = number of wind data sets input.

Then

$$u = u^C \delta \quad (15)$$

where u = final wind value. Note that for only one wind measurement, $n=1$, $u = u^m$.

The vertical wind is obtained by solving

$$\vec{\nabla} \cdot \vec{u} = 0 \quad (16)$$

in the finite difference form

$$v_{ij} = v_{i,j-1} + \Delta y_j \frac{(u_{i,j} - u_{i+1,j})}{\Delta x_i} \quad (17)$$

Typical wind fields for cut and fill sections calculated with this approach are presented in Figs. 1 and 2. Note that the flow smoothly traverses boundary corners. Local separated rotational flow regions are not established as might be encountered under actual flow conditions.

The cell structure of EXPLOR may be input manually or automatically calculated by the code. In either case, once the grid is fixed, the appropriate cells are determined to be terrain cells (i.e., ground). This is done by determining what portion of each cell is really underground. If the fraction exceeds one-half, the cell is set to an inert configuration in which it does not interact with the rest of the cells.

The source used in EXPLOR is a unit source in which the total quantity of a generalized pollutant sums to 1.0

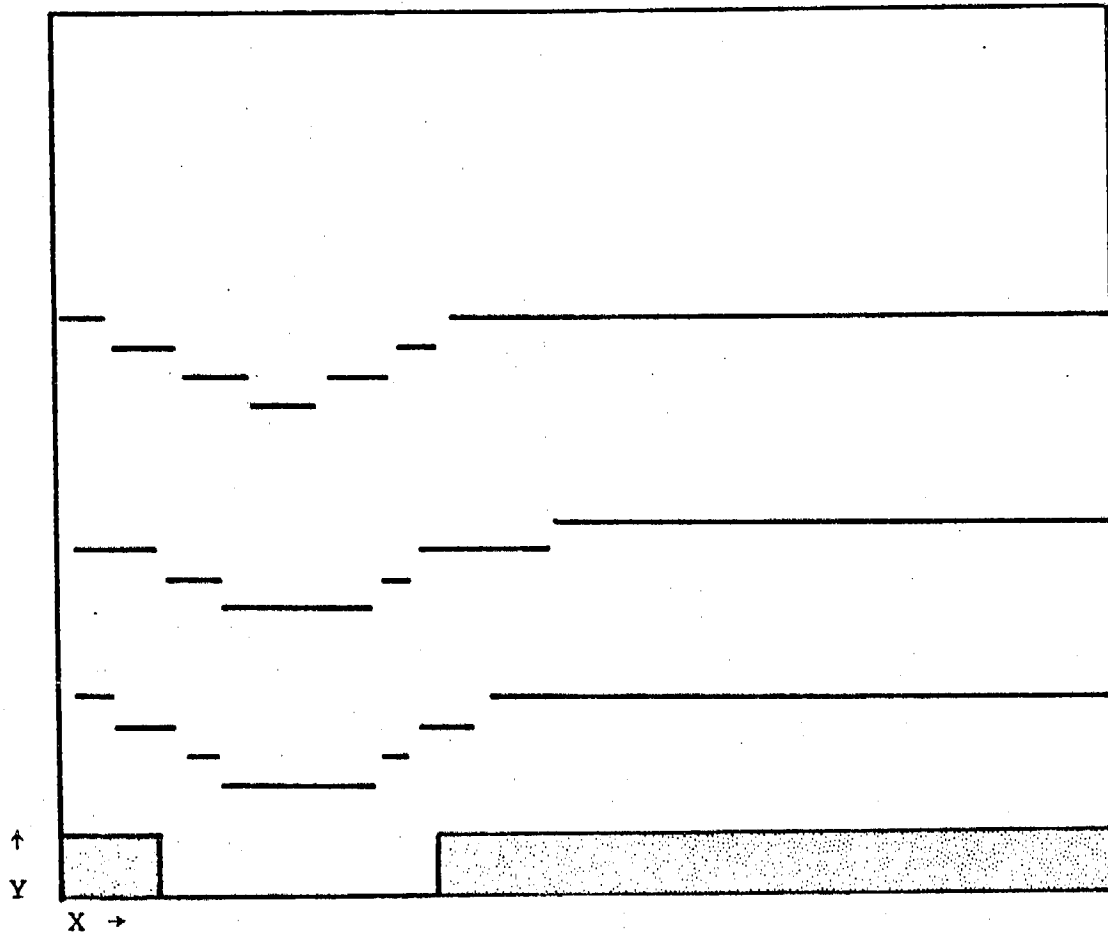


Figure 1 Windfield streamlines over cut section

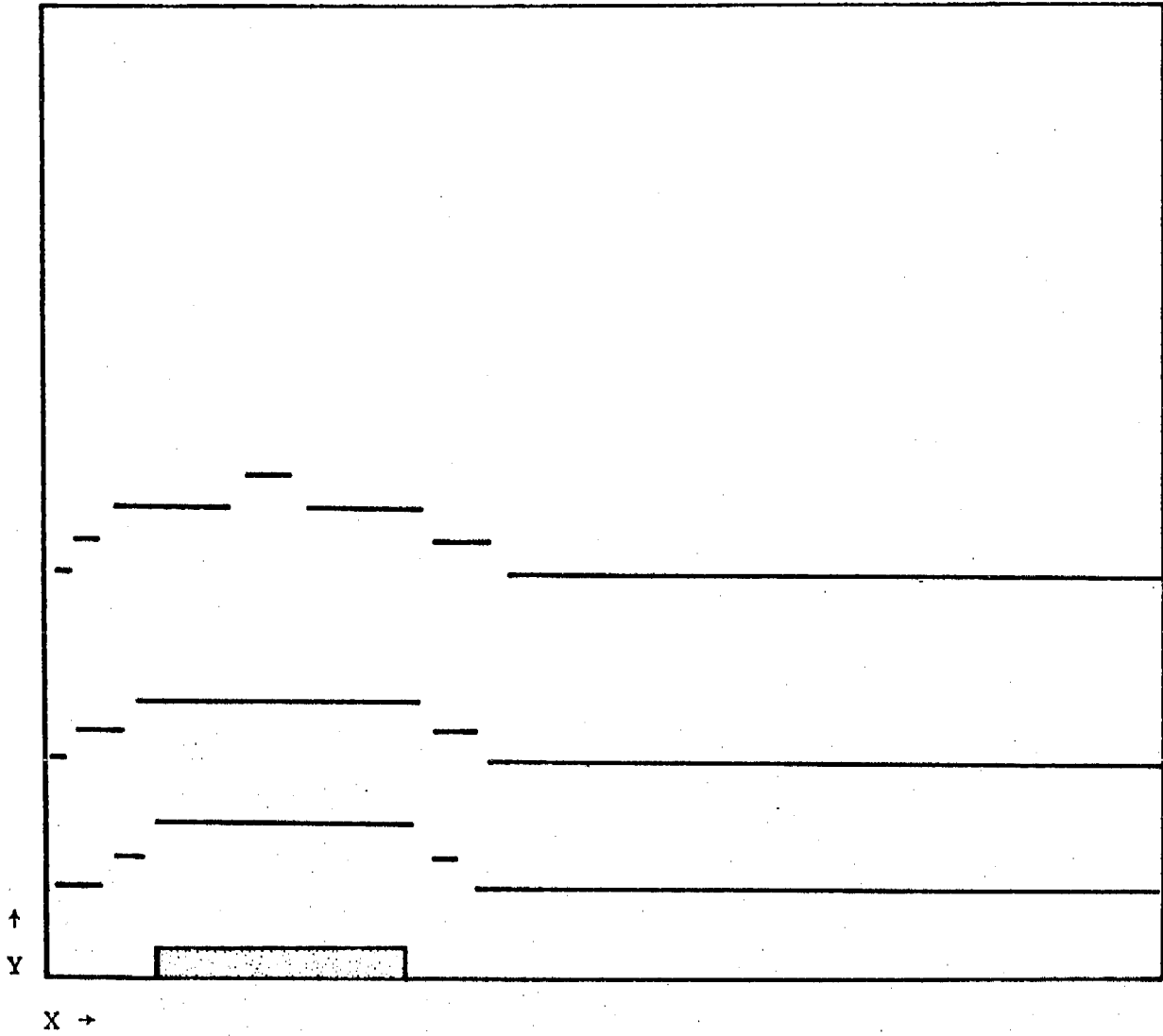


Figure 2 Windfield streamlines over fill section

at the problem's end. This results in normalized concentrations which are then scaled by the pollutant type, number of vehicles, emission factor, etc.

The source is introduced equally to every cell directly above the freeway. Generally the vehicles are in motion and mix the pollutant thoroughly in the source region (mixing cell). For this reason, the standard mode in EXPLOR is to force the concentrations in the mixing cell to be equal. This is done by an averaging process. If desired, the mixing option may be removed via input. This results in increasing concentrations across the freeway but has little effect at larger distances.

The theory regarding the zoning in EXPLOR is a compromise between economy and accuracy. To be at an optimum, each cell should be a square equal in size to all other cells. In reality, the cells directly above the freeway are taken to be equal sized rectangles, but the dimensions away from the road are tapered in a constant ratio. This allows a reasonable number of cells to cover an area large enough to be of interest. Because of inherent numerical stability considerations, the ratio, R , is preferably held to

$$0.75 \leq R \leq 1.25$$

Depending on circumstances, valid results may be obtained even when these restrictions are not obeyed.

4. THE EXPLOR CODE

In order to facilitate the flow of the main body of the report, as well as to provide a handy guide for the user, the complete listing of the 2-D EXPLOR code is located in Volume II. For the same reasons, a detailed manual for the running of the code is also given in Volume II.

A flow chart, which gives an overview of the code is shown in Figure 3. The sequence of operations is clearly shown and in combination with Appendices A and B thoroughly describes the code.

2-D EXPLOR has been extended in a crude form to three dimensions. Because of a lack of 3-D data, this version of the code could not be evaluated. A description of this version of EXPLOR is given in Appendix A, and a sample calculation is found in Appendix B.

4.1 VALIDATION

4.1.1 Data

The data for the validation were obtained from the California Air Resources Board (ARB) for four locations in the Los Angeles Area. These locations are:

- Fill - San Diego Freeway at 122nd
- At Grade - San Diego Freeway @ Weigh Station
- Cut I - Harbor Freeway at 146th

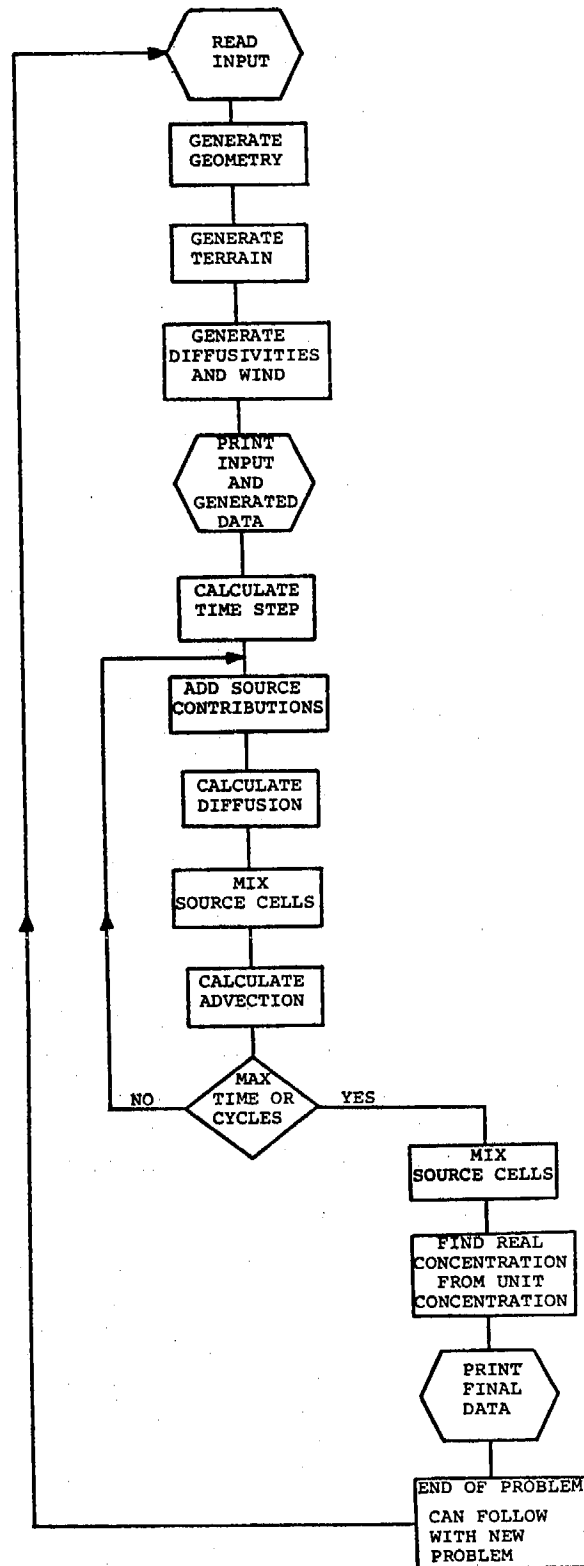


Figure 3 EXPLOR flow chart

Cut II - Santa Monica Freeway

The geometries for these locations are shown in Figure 4.

These sites were selected to be particularly "clean" in the sense that surrounding terrain was level and generally uncluttered. Hence, 2-D codes are appropriate. The at-grade, fill, and first cut section are actually located between open fields (within the highway corridor). The second cut section (cut 2) is in a primarily residential area, and is flanked on both sides by one or two family residential housing. Note that a mixing cell height of 10 ft was utilized in all calculations.

Three basic traffic parameters determine the source strength for a calculation. There is the traffic rate (in vehicles per hour), the amount of heavy duty traffic (in percent of total traffic), and mean vehicle speed (in mph). The last two are used to select the emission factor of a given pollutant (gm/mile/vehicle) from curves developed by the California Division of Highways, [7] which predict the emission factors (gm/mi) as a function of year, average route speed, and percentage of heavy duty traffic. The factors decline with each future year as more and more vehicles are operating with pollution controlled engines.

The Division of Highways carbon monoxide emission factors for a 5 percent heavy-duty vehicle mix are shown in Fig. 5. Similar curves are available for 0, 10, 15 and 20 percent heavy-duty vehicle mixes. These have been generated specifically for freeway driving with a computational methodology similar to Sigworth, [8] whose EPA emission factors are more appropriate for city driving.

4.1.2 Methodology

The validation study is primarily directed at deter-

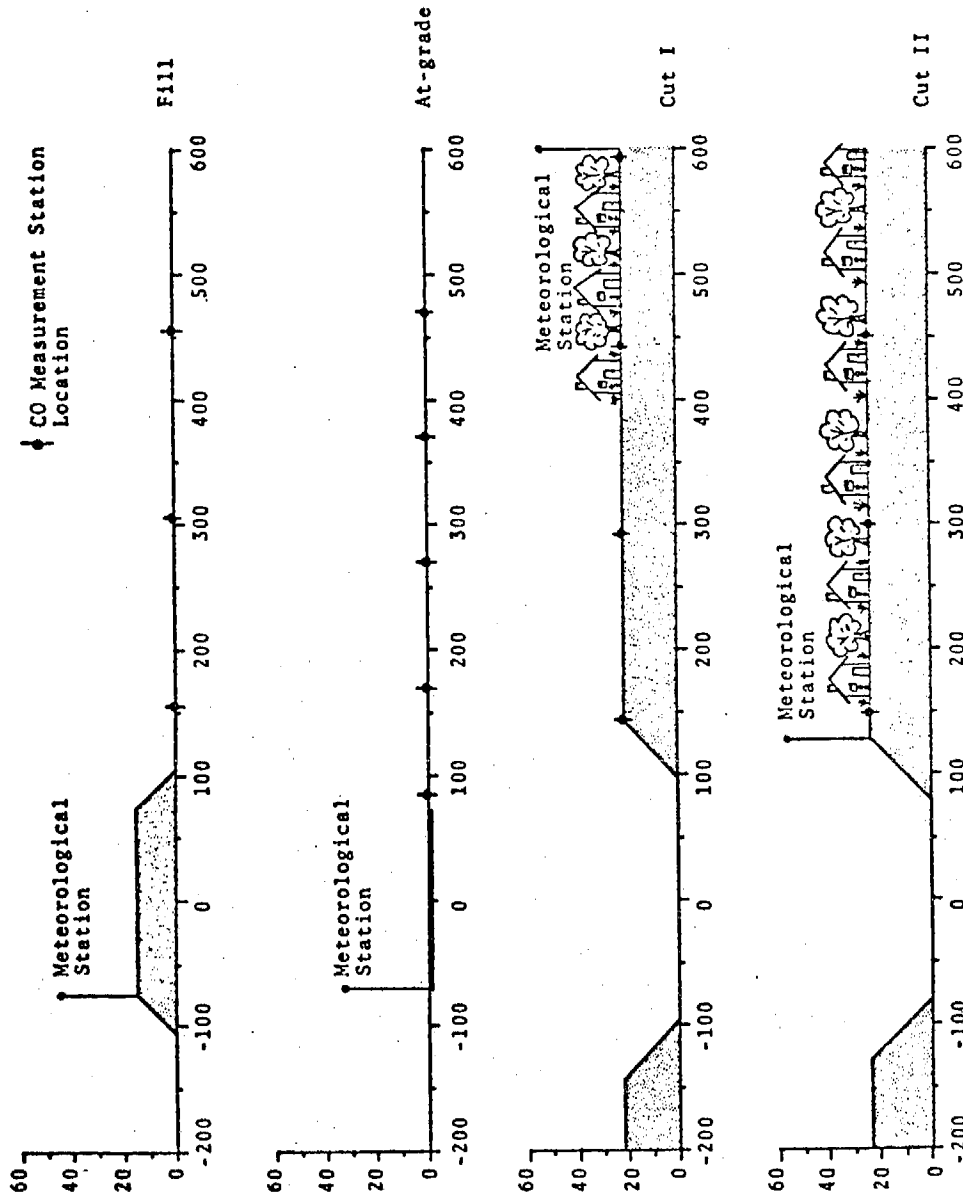


Figure 4 Schematic illustration of test sites utilized in the measurement portion of the validation study. The CO measurement stations are denoted for each site. All dimensions are in feet.

EMISSION FACTORS FOR CARBON MONOXIDE VS AVERAGE ROUTE SPEED ON FREEWAYS

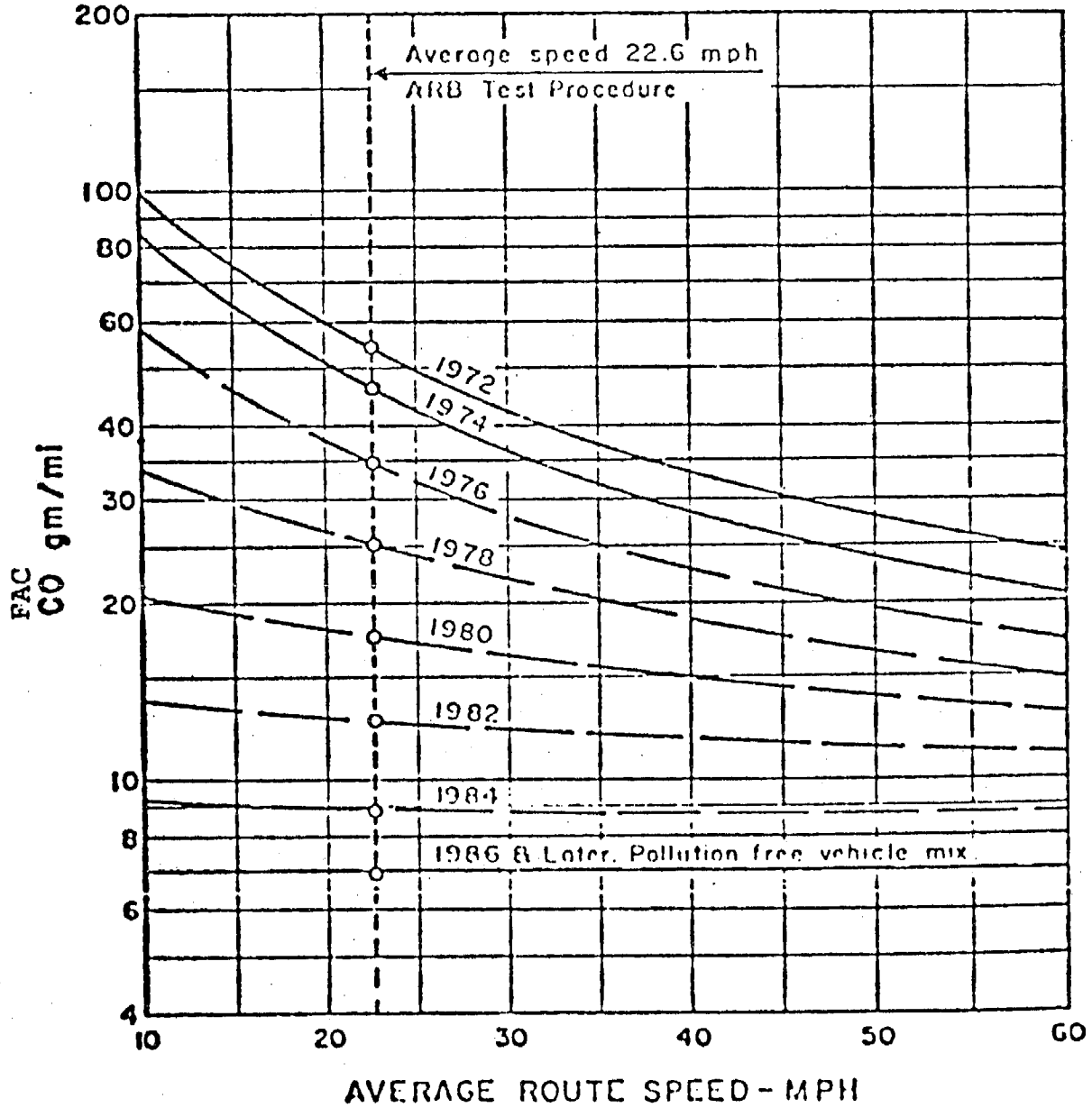


Figure 5 Curve for determination of CO emission factor for 5 percent heavy duty traffic (grams per car per mile)

mining the predictive accuracy of EXPLOR for ground level, off-roadway pollutant concentrations. These validations consist of CO concentrations measured over half hour and hourly intervals at various positions in the immediate and far vicinity of the roadway (see Fig. 4 for off-roadway, ground level positions). The concentration was measured to the nearest ppm. In addition to the CO measurements, the input data included traffic counts (in both directions), local wind velocity (to the nearest knot and compass heading ($22\frac{1}{2}^\circ$)), and Pasquill stability class (based on the observational method outlined in Ref. 9). An occupancy factor was also reported, in some cases, that permits calculation of average traffic speed. The heavy duty vehicle percentage was taken to be 5 percent (based on average traffic volume at each location, but it was not measured for each case).

Given the nature of the input data, it was felt necessary to impose a consistent set of qualifications for cases to be used in the EXPLOR validation program. This is necessary to minimize the number of cases that contain anomalous results due to unsteady meteorological conditions and/or three-dimensional effects. These qualifications are as follows:

- Only complete sets of hour-average data were utilized (including upwind background concentrations).
- Wind direction within ± 1 compass heading ($22\frac{1}{2}^\circ$) of previous or subsequent hour. (All cases of 0° (parallel) winds were also ignored).
- Pasquill stability class within ± 1 of previous or subsequent hour.
- Ceiling above 10 ft.

- CO measurements far from road must show finite gradient over a 200 ft distance if CO levels are above upwind background.

Under these restrictions, it was possible to select 41 hour-average cases, consisting of 137 CO measurements* obtained during daylight hours on 14 different dates in 1972. The majority of the data was for C and D stability conditions but 28 of the data points were at B stability and 10 points were obtained under A stability conditions. These input data are presented in Tables 4 - 7.

The comparison of EXPLOR predictions to measured CO concentrations, assuming measured values to be correct, was accomplished by computing the mean error, μ , and root mean square error, σ , for each case. These are defined by

$$\mu = \frac{\sum_{i=1}^N \epsilon_i}{N}, \quad \sigma = \sqrt{\frac{\sum_{i=1}^N \epsilon_i^2}{N}} \quad (18)$$

where

ϵ_i = error = $(C_{\text{calc}} - C_{\text{meas}})$ for the i^{th} point

C_{calc} = calculated concentration

C_{meas} = measured concentration

N = number of points in sample

* This includes 14 roadway-edge data points (see discussion in subsequent section).

TABLE 4
Input Data "At-grade" Section

(Off-highway measurements taken at distances of 85, 170, 270, 370, and (in cases of 5 data points) 470 ft from centerline)

Date	Hour	Wind Speed (mph)	Wind Angle (deg)	Stability Class	Traffic Volume (cars/hr)	Avg. Traffic Speed* (mph)	Data Points
4/5	7-8	3.45	39 1/2	B	13428	40	4
4/5	9-10	8.05	39 1/2	B	9032	60	4
4/5	11-12	8.05	39 1/2	B	8339	60	4
4/5	12-13	10.35	39 1/2	C	7937	60	4
4/5	13-14	11.5	39 1/2	C	8488	60	4
4/12	9-10	10.35	39 1/2	C	9246	60	5
4/13	7-8	17.25	39 1/2	D	13918	40	5
4/13	8-9	19.55	39 1/2	D	11830	40	5
4/13	9-10	12.65	39 1/2	C	9246	60	5
4/13	10-11	13.8	39 1/2	D	8497	60	5
4/13	11-12	14.95	39 1/2	D	8447	60	5
4/13	12-13	16.1	39 1/2	D	7887	60	5
4/14	7-8	3.45	84 1/2	B	13918	40	5
4/14	10-11	8.05	50 1/2	B	8497	60	5

*Average speed not recorded in the sets of data. Rush hour traffic has been assumed to move at 40 mph, with nominal traffic at 60 mph.

TABLE 5

Input Data - "Fill" Section

(Off-highway measurements taken at distances of 155, 305, and 455 ft from center line)

Date	Hour	Wind Speed (mph)	Wind Angle (deg)	Stability Class	Traffic Volume (cars/hr)	Avg. Traffic Speed* (mph)	Data Points
10/3	13-14	9.2	57	C	9403	60	3
10/3	15-16	9.2	57	C	14669	45	3
10/4	13-14	12.65	79 1/2	C	10078	60	3
10/4	14-15	13.8	57	D	12107	60	3
10/4	15-16	12.65	34 1/2	C	14954	60	3

TABLE 6

Input Data - Cut I Sections

(Off-highway measurements at 143, 293, 443, and 593 ft from center line)

Date	Hour	Wind Speed (mph)	Wind Angle (deg)	Stability Class	Traffic Volume (cars/hr)	Avg. Traffic Speed (mph)	Data Points
8/2	16	5.75	22 1/2	A	11484	53	2
8/9	11	5.75	22 1/2	A	6458	56	4
8/9	12	5.75	22 1/2	A	5946	60	4
8/9	14	8.05	67	B	7539	60	4
8/9	16	8.05	67	B	11792	54	4

* All indicated speeds over 60 mph were set at 60 mph.

TABLE 7

Input Data - Cut II Section

Date	Hour	Wind Speed (mph)	Wind Angle (deg)	Stability Class	Traffic Volume (cars/hr)	Avg. Traffic Speed* (mph)	Data Points
5/4	8	4.6	35	D	16518	40	2
5/4	9	3.45	35	D	14017	60	2
5/4	10	4.6	57 1/2	D	13288	60	2
5/9	8	3.45	80	B	15754	40	3
5/9	9	3.45	57 1/2	C	14943	60	3
5/15	9	3.45	80	D	14232	60	5
5/16	7	3.45	80	D	16816	40	2
5/16	8	3.45	80	D	16196	40	3
5/16	9	3.45	57 1/2	C	14714	60	3
5/17	7	4.60	35	D	16992	40	2
5/17	8	3.45	35	D	16452	40	2
5/17	9	3.45	57 1/2	D	14200	60	2
5/17	10	3.45	35	D	13219	60	2
5/19	7	3.45	80	C	16349	40	2
5/19	8	5.75	80	D	15491	40	2
5/19	9	4.6	80	D	14250	60	2
5/19	10	6.9	80	D	13469	60	2

*All indicated speeds over 60 mph were set at 60 mph.

4.1.3 Basic Results

Considering each freeway location separately, the EXPLOR predictions yielded the following results:

TABLE 8
Basic EXPLOR Validation Results

Section	Mean Error μ , ppm	Root Mean Square Error (ppm)
At-grade (65 points)	(-.48)	(1.32)
Cut I (18 points)	(-.23)	(.60)
Cut II (39 points)	(-.68)	(1.45)
Cut I and II (57 points)	(-.54)	(1.24)
Fill (15 points)	(-.35)	(1.02)
All Sections (137 points)	(-.49)	(1.26)

Scatter plots showing the disposition of measured versus calculated concentrations are given in Figs. 6, 7, and 8. Note that two plots are shown for the at-grade section (8a and 8b), to show the effect of neglecting the roadway edge measurements.

4.1.4 Estimate of Experimental Error

The data sample was not large enough to provide enough duplicate or near-identical test conditions to ascertain the repeatability of the experimental observations. However, it is possible to determine the sensitivity of the EXPLOR pre-

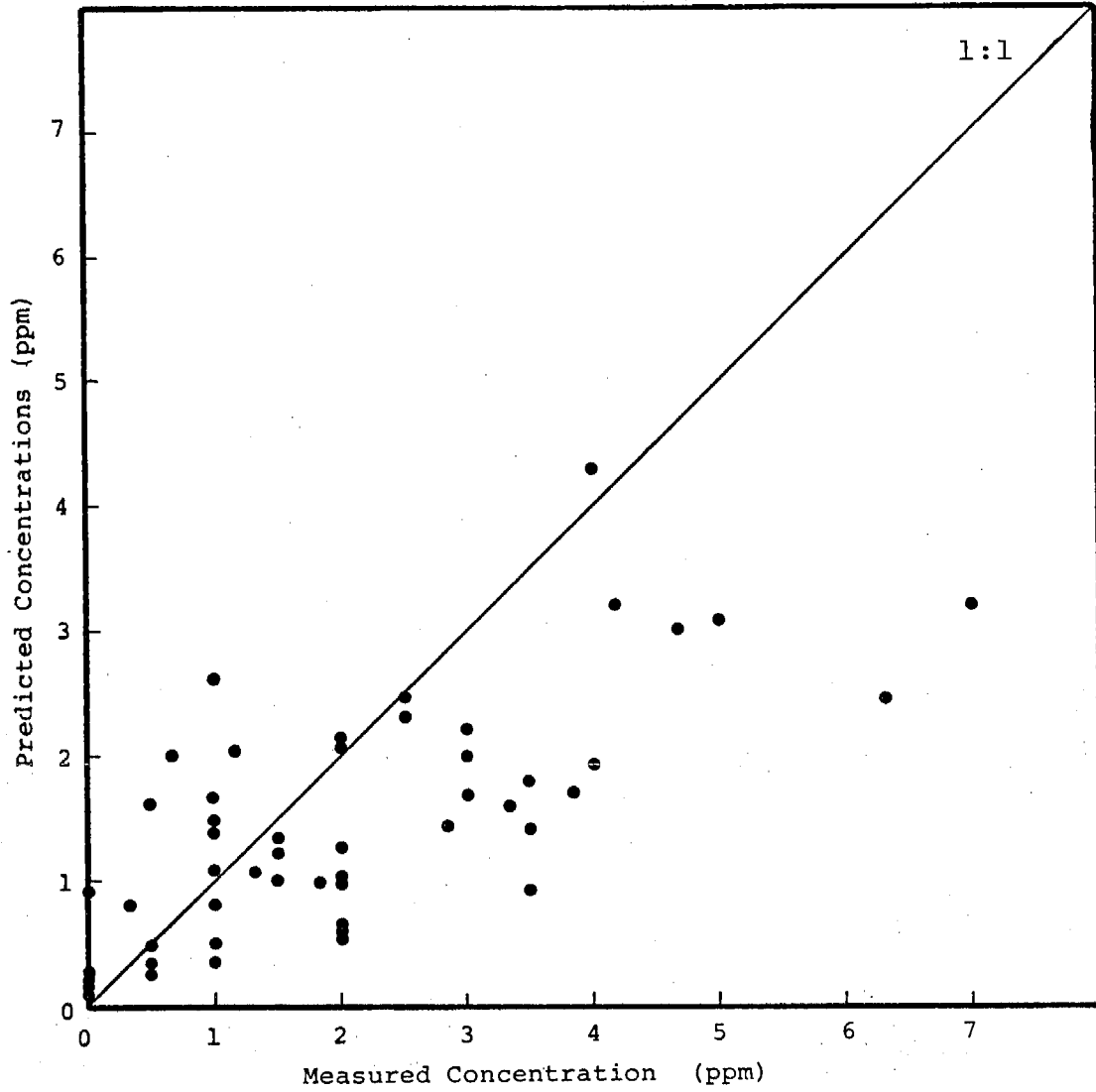


Figure 6. Scatter plot of EXPLOR predictions versus measured CO concentrations. Cut I and II sections.

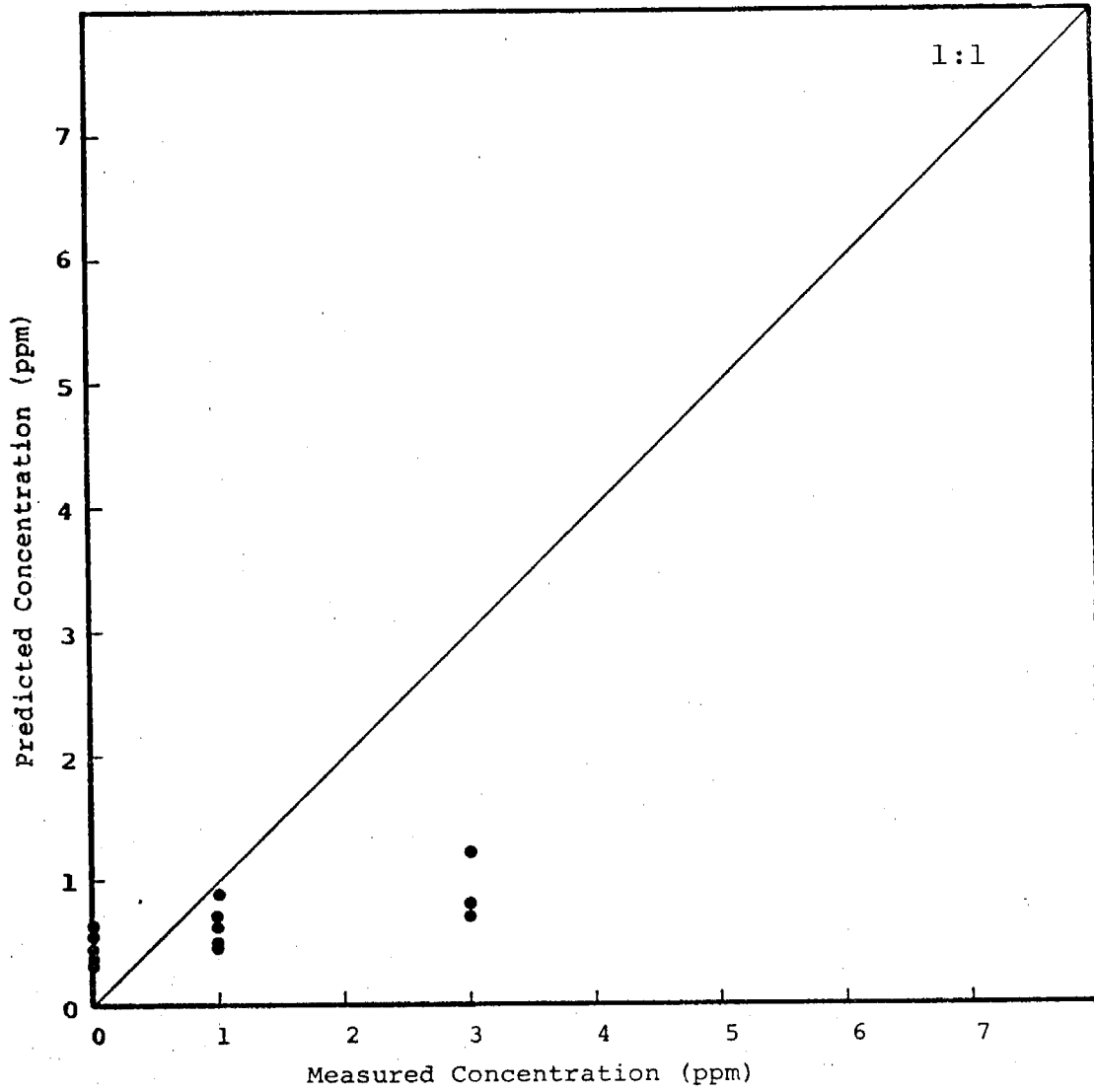


Figure 7 Scatter plot of EXPLOR predictions versus measured CO concentrations. Fill section.

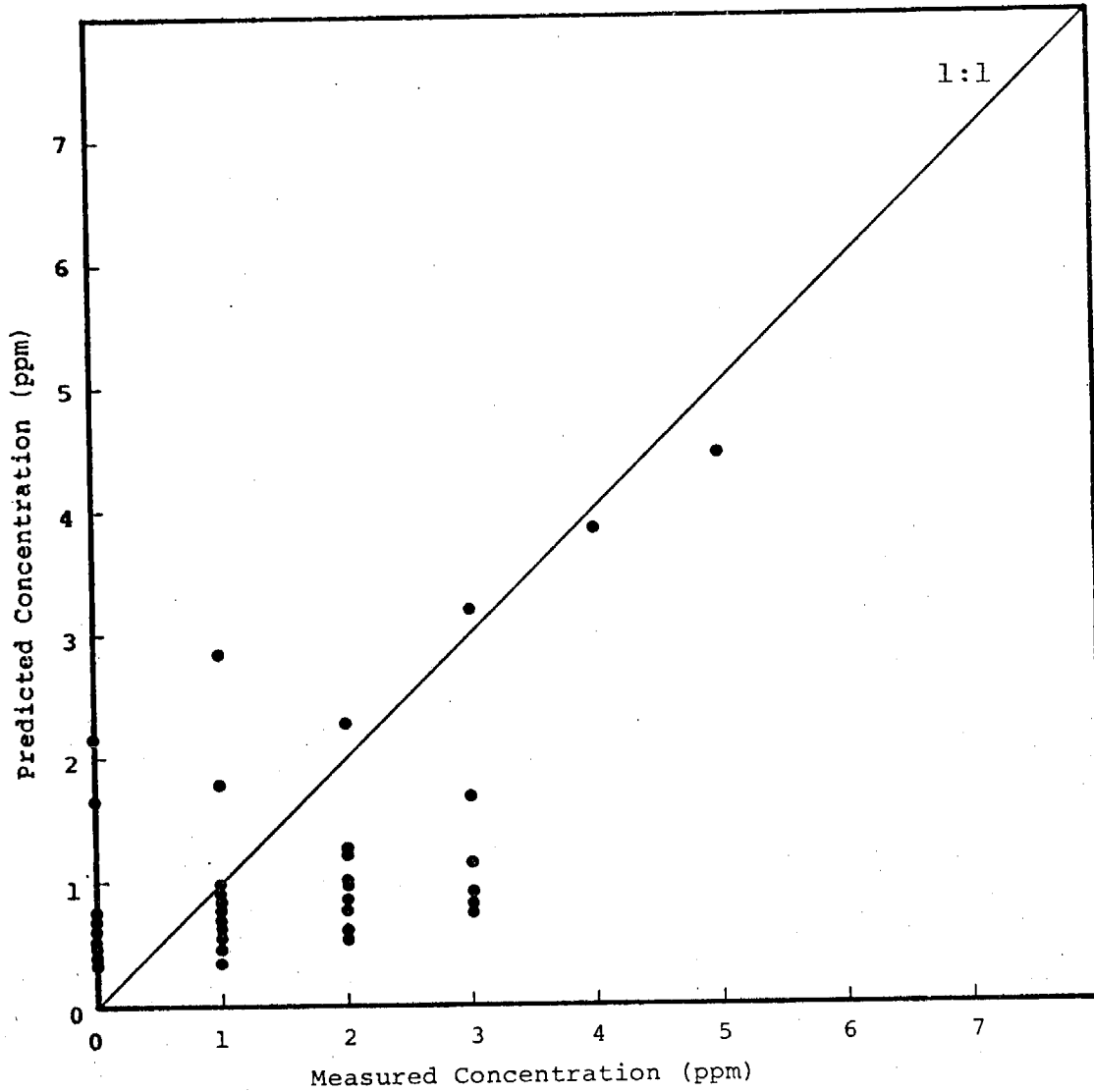


Figure 8A Scatter plot of EXPLOR predictions versus measured CO concentrations. At grade section (not including road edge measurements).

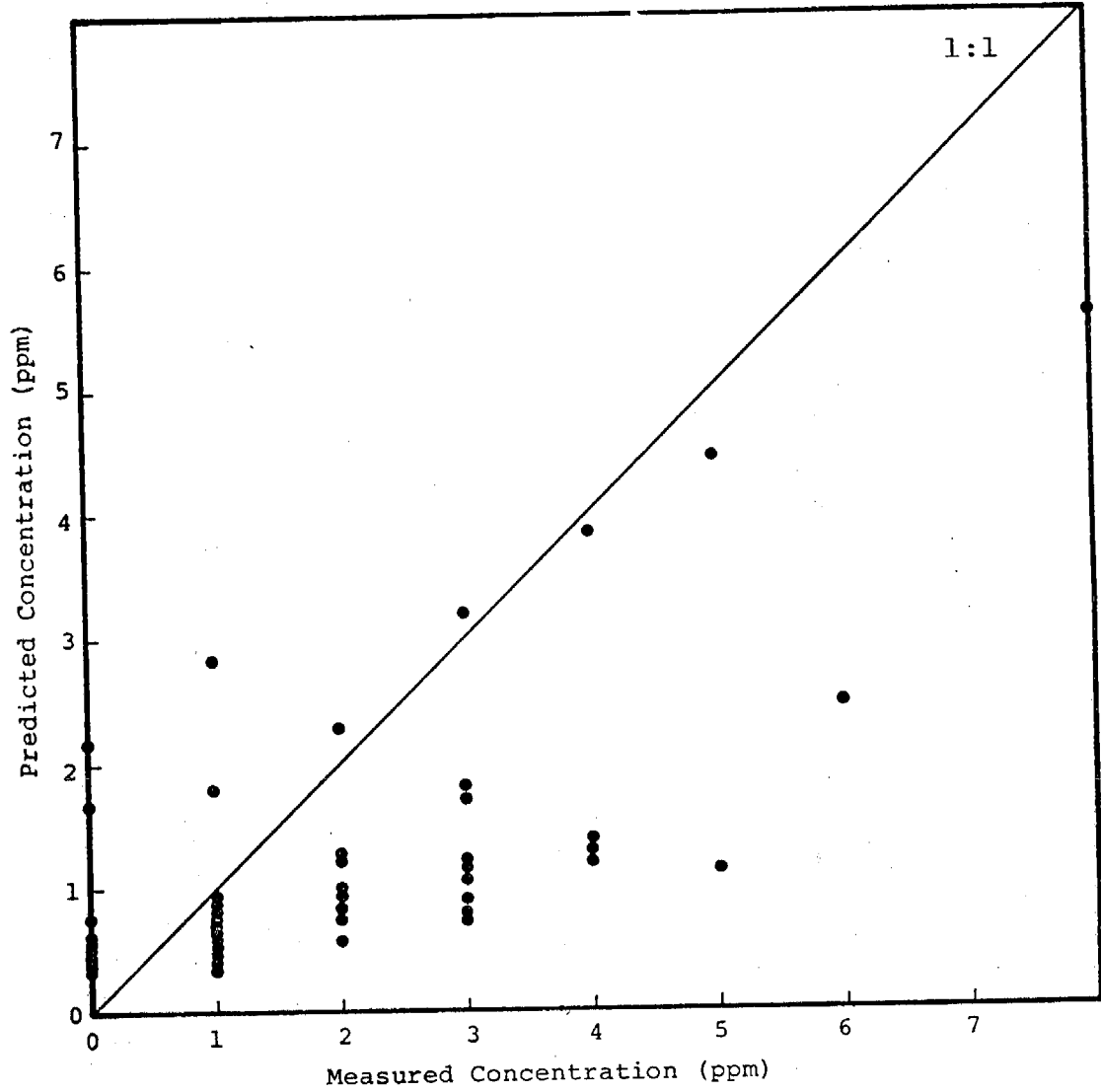


Figure 8B Scatter plot of EXPLOR predictions versus measured CO concentrations. At grade section (including road edge measurements).

dictions to changes in the input that reflect the most likely sources of error. These sources and the variations studied are

- Heavy duty traffic volume, ± 3 percent about the 5 percent nominal value.
- Traffic speed, ± 5 mph.
- Wind angle, $\pm 10^\circ$ about nominal value.
- Stability class, ± 1 about nominal identification.

By combining these variations to give maximum and minimum predictions of the ground level CO concentration, errors due to inherent inaccuracies in the input data can be calculated. Typical results for five cases are given in Fig. 9. The mean error band for these five minimum-maximum predictions is ± 1.48 ppm. Of this error, approximately 70 percent is due to ± 1 stability class changes, 20 percent to ± 3 percent HD traffic and ± 5 mph in traffic speed, and 10 percent due to wind angle errors. If we presume that the stability class effects can be estimated by taking the total variation to be 1/3 that of the ± 1 class variation results, the error band width due to data input inaccuracies is ± 0.8 ppm. Finally, if the ± 0.5 ppm error in the CO measurements is added to this figure, we arrive at an estimated error band for the validation study of

$$\epsilon = \pm 1.3 \text{ ppm} \quad (19)$$

Thus, the root mean square of the present study ($\sigma = 1.26$ ppm), including the roadway edge measurements, falls within this band-width. We conclude, therefore, that the EXPLOR model is validated to within the accuracy of the experimental data.

It must be noted that for all four sites the mean error is negative, indicating that EXPLOR predictions are generally

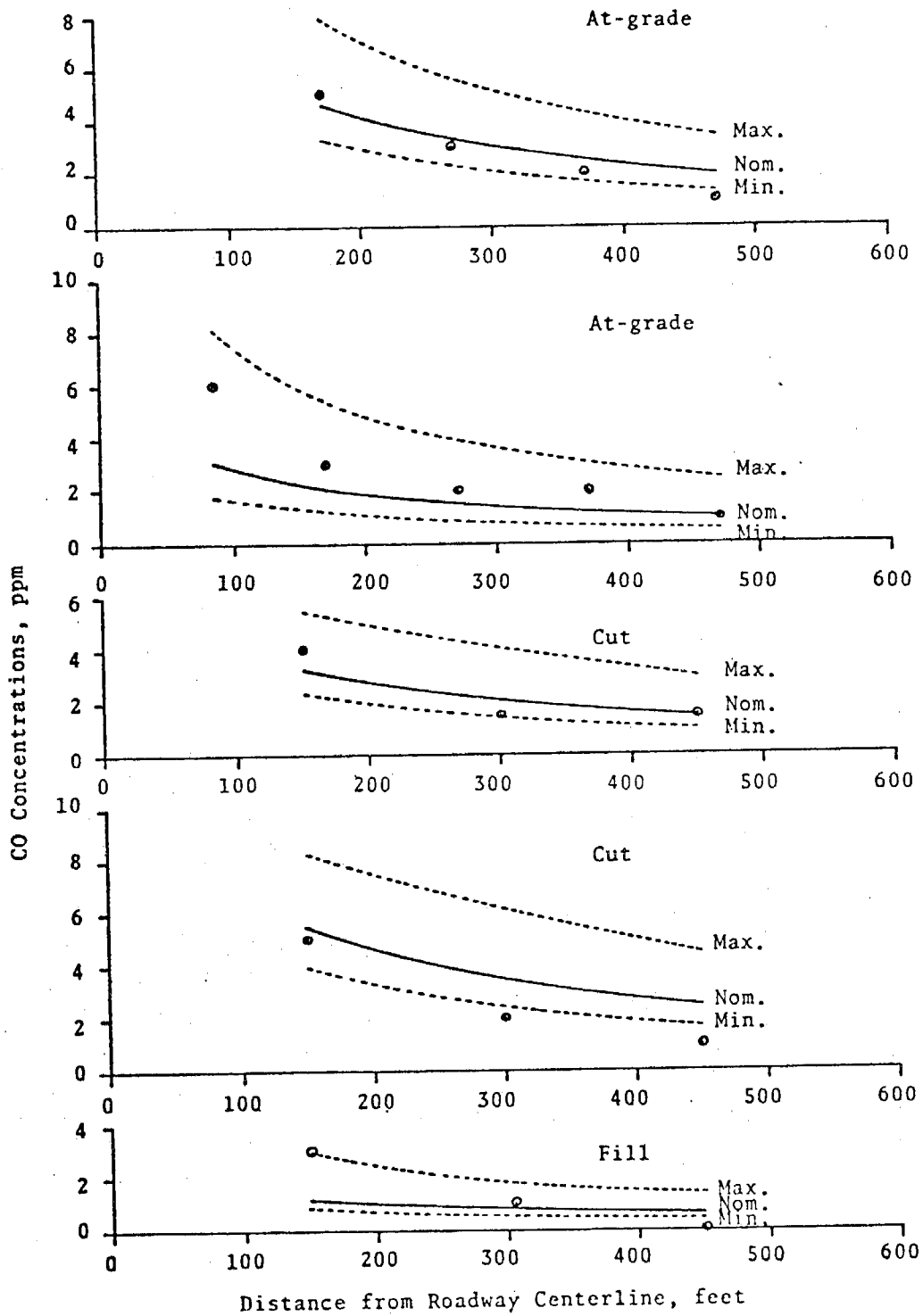


Figure 9 Comparison of maximum, nominal, and minimum ground level CO concentrations predicted by EXPLOR due to variations in input conditions. Experimental measurements for these cases are indicated by circles.

low. It is felt that this is due primarily to low concentrations predicted for the roadway and the values used for the diffusivities. Both are mentioned in Section 2 as areas requiring further study.

4.1.5 Sources of Error

Roadway Edge Measurements -- The single most identifiable trend in the data is the apparent overestimation of turbulent mixing processes at the roadway with the present mixing layer model, leading to consistently low predictions of CO at the downwind highway edge. This is most apparent in the results for the at-grade section, wherein the first CO measurement was actually taken at this position. (The other sections' closest positions were at the top of the cut or bottom of the fill, removed by over 45 feet from the roadway edge (see Figure 4).)

Analysis of the at-grade section data indicates the mean error at the road edge position was (-2.56) ppm, with a root mean square error of (2.68) ppm. These are both much higher than the remainder of the data (i.e., 56 points, $\mu = (-.15)$ ppm, $\sigma = (.87)$ ppm), indicating that the roadway mixing model in EXPLOR should be modified to predict less mixing in the immediate vicinity of the roadway. The other nearest road measurements, summarized in Table 9, tend to support this conclusion.

Note that if the at-grade roadway edge position is excluded from our validation study (on the grounds that it is still strongly influenced by roadway conditions), the statistical comparison between prediction and measurement (128 points) is characterized by

$$\begin{array}{ll} \mu = (-.34) \text{ ppm} & \text{off-roadway results} \\ \sigma = (1.09) \text{ ppm} & 128 \text{ points} \end{array} \quad (20)$$

Cross-Wind Angle -- The EXPLOR predictions for the two cut locations were divided into cases with cross-wind angles greater or less than 45° . For this section, there was a marked increase in error at the high cross-wind angles. At these test sites (primarily cut II), the cross-wind angles did not correspond to a particular time of day so that a fair sampling of rush-hour and nominal traffic was obtained (see Tables 4 - 7). The mean and root mean square errors are shown in Table 10.

TABLE 9
EXPLOR Validation Results -
Near Roadway Versus Far Roadway
CO Measurement Stations

At-Grade Section:	85 ft(9 points)	170, 270, 370 and 470 ft (56 points)
μ , ppm	-2.56	-.15
σ , ppm	+2.68	+.93
Fill:	155 ft(5 points)	305 and 455 ft (10 points)
μ , ppm	-1.45	+.20
σ , ppm	+1.66	+.42
Cut I	143 ft(5 points)	293, 443, and 593 ft (13 points)
μ , ppm	-1.02	+.08
σ , ppm	+1.10	+.16
Cut II	150 ft(17 points)	300 and 450 ft (22 points)
μ , ppm	-1.56	0.00
σ , ppm	+1.95	+.87

TABLE 10
EXPLOR Validation Results for Different
Cross- Wind Angles

Error	High Cross-wind Angles, 90° - 45° (37 points)	Low Cross-wind Angles, 12° - 45° (20 points)
μ , ppm	- .84	+ .03
σ , ppm	+1.41	+ .84

Added roughness effects due to the traffic and some degree of flow channeling down the cut section may produce a local air flow significantly different from the relatively smooth mean flow computed by the EXPLOR wind field and diffusivity subroutines. Unfortunately, the data samples at other locations were not adequate to attempt to separate out this effect. Further experimental results are necessary to reach any firm conclusions on cross-wind angles effects.

Traffic Volume -- The primary sites in this study, the cut II and the at-grade sections, provided the opportunity of comparing EXPLOR predictions to actual measurements during rush hour (7:00 - 9:00 am) and normal (9:00 am - 4:00 pm) traffic conditions. At rush hour, traffic moves slower (~ 40 mph) and the emission factors for each automobile are predicted to rise over the normal 60 - 70 mph traffic. The slower, more dense rush hour traffic may also disturb the wind flow-field in a different manner than the normal traffic pattern. Our EXPLOR predictions yield the following results:

TABLE 11
EXPLOR Validation Results -
Rush Hour Versus Normal Traffic

Error	Rush Hour	Normal Traffic
Cut II μ , ppm σ , ppm	- .71 +1.69 } 18 points	- .65 +1.19 } 21 points
At-grade (off-roadway) μ , ppm σ , ppm	+ .21 +1.04 } 16 points	- .29 + .90 } 40 points

These results are clearly indicative of a trend towards error in the off-roadway ground level concentrations under rush hour conditions. It should be noted, however, that measured concentrations are approximately 30 - 40 percent different during the rush hour period. If we presume the accuracy of the total measuring system (in ppm) is proportional to the magnitude of the emitted pollutant, this would account for the increase in the standard deviation of the predictions (from the measurements). The induced diffusivity field (off the roadway) due to slower roadway traffic may not be properly treated in the EXPLOR model and/or the emission factors under freeway rush hour conditions may be simply less accurate. Based on the validation results for the measurements nearest the highway, it would appear that first priority should be given towards improving the treatment of these automobile-roadway induced diffusivity fields. However, the indeterminacy of traffic speed under rush-hour conditions may also be an important factor.

Stability Class -- Four stability classes were included in the data sample (A - D). The validation cases were grouped according to stability class, and the associated mean and root mean square errors are as follows:

TABLE 12
EXPLOR Validation Results -
Atmospheric Stability

Error	Pasquill Stability Class			
	A (10 pts)	B (31 pts)	C (36 pts)	D (51 pts)
μ , ppm	-.22	+ .07	- .75	- .33
σ , ppm	+.60	+0.89	+1.26	+1.15

With the exception of the class A results, no significant departures from the overall off-roadway results ($\mu = -.34$ ppm and $\sigma = 1.09$ ppm) is apparent. The class A sample, however, is too small to conclude that the EXPLOR model is superior under the most unstable conditions. (Moreover, A stability conditions result in minimal CO concentrations, so that absolute errors should be smaller.)

4.2 DISCUSSION

EXPLOR is a major improvement in predicting off-roadway pollution concentrations. Rather than relying on the Gaussian model approach, the realistic transport of pollutants is calculated. This is a great improvement because the introduction of complex terrain features is now allowed.

The wind field is calculated by the code, based on the terrain, another major step forward. As mentioned in the January 1973 interim report, in an EPA study for at grade and cut roadways, the best competing Gaussian model gave approximately five times the mean error and three to four times the root mean square error that EXPLOR with the MRI diffusivity prescription did.

EXPLOR can be used for a number of roadway types including at-grade, cuts, fills, bridges and viaducts. The latter two allow the pollutant to be mixed with fresh air introduced from below the roadway.

Other details of the code and its validation have been described above.

REFERENCES

1. Crowley, W.P., "Numerical Advection Experiments," Monthly Weather Review, (January 1968) Volume 1.
2. Lantz, R. B., Coats, K. H., and Kloepfer, C. V., "A Three-dimensional Model for Calculating the Spread and Dilution of Air Pollutants," Proceedings of the Symposium on Air Pollution, Turbulence and Diffusion, New Mexico, December 1971.
3. DeMarrais, G. A., "Vertical Temperature Difference Observed over an Urban Area," Bull. Amer. Meteorol. Soc., 42, 8, 548-554
4. Smith, T. B., and Howard, S. M., "Methodology for Treating Diffusivity," (September 1972) report to Systems, Science and Software by Meteorology Research Inc.
5. Smith, T. B., and Niemann, B. L., "Shoreline Diffusion Program: Oceanside, California, Vol. 1, Technical Report," Contract No. DA 42-007-AMC-180 (R), (1969), Final report by Meteorology Research Inc. to Deseret Test Center, Ft. Douglas, Utah.
6. Taylor, R. J., Warner, J., and Bacon, N. E., "Scale Length in Atmospheric Turbulence as Measured from an Aircraft," Quart. J. Roy. Met. Soc., 96, pp. 750-755.
7. Beaton, J. L., Skog, J. B., Shirley, E. C., and Ranzieri, A. J., "Mathematical Approach to Esti-

mating Highway Impact on Air Quality," (July 1972) (emission factors in appendix).

8. Sigworth, H. W., "Estimates of Motor Vehicle Emission Rates - - 1971," cited in Beaton, et al.
9. Pasquill, F., Atmospheric Diffusion, D. Van Nostrand Co., Ltd., New York, (1962).
10. Sutton, O. G., Micrometeorology, McGraw-Hill, New York (1953).
11. Sutton, O. G., and Pasquill, F., Atmospheric Diffusion, D. Van Nostrand, New York (1962).

PUBLICATIONS

Kirsch, J. W., Mason, B. F., Teuscher, L. H.,
"Validation of a Highway Air Pollution Model" Presented
at the 1973 Summer Computer Simulation Conference, Montreal,
Canada.

Versions of EXPLOR are currently in use by:

1. Scott Laboratories
Plumsteadville, Pa.
2. Oregon Division of Highways
Salem, Oregon

GLOSSARY OF SYMBOLS

C	Pollutant concentration (ppm)
C_{calc}	Calculated concentration (ppm)
C_{meas}	Measured concentration (ppm)
F	Flux (quantity - ft/sec)
i	Spatial index
k	Diffusivity (ft ² /sec)
\underline{k}	Turbulent diffusivity tensor
ℓ	Turbulence scale length (ft)
n	Temporal index
N	Number of points in sample
p	Stability class parameter
S	Emission source strength (unity)
t	Time (sec)
u	Local wind speed (ft/sec); horizontal wind speed (ft/sec)
\bar{u}	Mean wind velocity (ft/sec)
u'	Turbulent fluctuation velocity at which turbulent energy is maximized (ft/sec)
u^c	Calculated velocity (ft/sec)
u^m	Measured velocity (ft/sec)
v	Vertical wind speed (ft/sec)
x	x (horizontal) dimension (ft)
y	y (vertical) dimension (ft)
z	Height above road (ft)
z_0	Reference height (ft)
α	Constant in iteration procedure, >1
δ	Least squares parameter
Δx	Distance from cell boundary to cell boundary in x direction (ft)
Δx^a	Distance from cell center to cell center in x direction (ft)

Δy	Distance from cell boundary to cell boundary in y direction (ft)
ϵ_i	Error at i^{th} point
$\underline{\lambda}$	Potential coefficient tensor
μ	Mean error
σ	Root mean square error
σ_ϵ	Mean wind vane fluctuation (radians/sec)
Σ	Summation symbol
ϕ	Velocity potential (ft ² /sec)
Ω	Dummy variable

FOR APPENDIX A ONLY

C	Concentration
F_x', F_y', F_z'	Flux
K	Eddy diffusivity tensor
t	Time
x, y	Dimensions in plane of ground
z	Vertical dimension
u, v, w	Wind velocities x, y, z directions
$\bar{u}, \bar{v}, \bar{w}$	Mean velocity field
u_f', v_f', w_f'	Turbulent flux velocities

APPENDIX A

THREE-DIMENSIONAL EXPLOR

The 3-D EXPLOR code uses basically a three-dimensional form of the above 2-D EXPLOR equations, but is unique in its use of Lagrangian mass points (called particles) representing pollutant mass.

Changes in particle position are calculated to simulate pollutant mass transport due to both advection and diffusion as specified by the turbulent atmospheric diffusion equation.

The equation describing turbulent atmospheric diffusion,

$$\begin{aligned} \frac{\partial c}{\partial t} = & - \bar{u} \frac{\partial c}{\partial x} - \bar{v} \frac{\partial c}{\partial y} - \bar{w} \frac{\partial c}{\partial z} + \frac{\partial}{\partial x} K_x \frac{\partial c}{\partial x} \\ & + \frac{\partial}{\partial y} K_y \frac{\partial c}{\partial y} + \frac{\partial}{\partial z} K_z \frac{\partial c}{\partial z} , \end{aligned} \quad \text{A-1}$$

equates the time rate of change of concentration c , $\partial c / \partial t$, to advective rate of change of c ,

$$- \bar{u} \frac{\partial c}{\partial x} - \bar{v} \frac{\partial c}{\partial y} - \bar{w} \frac{\partial c}{\partial z} ,$$

due to the mean velocity field ($\bar{u}, \bar{v}, \bar{w}$,) plus the divergence of the turbulent flux with the position dependent eddy diffusivity (K_x, K_y, K_z)

$$\frac{\partial}{\partial x} K_x \frac{\partial c}{\partial x} + \frac{\partial}{\partial y} K_y \frac{\partial c}{\partial y} + \frac{\partial}{\partial z} K_z \frac{\partial c}{\partial z} .$$

Considering general wind fields, there is no assumption that the x-direction diffusion term is negligible. Discussions of the derivation of this equation are given in several sources, e.g., Sutton [10] and of the applications to atmospheric diffusion in Sutton and Pasquill [11].

The diffusion equation can be rewritten in a suitable form by use of the following definitions. The turbulent flux, for example, in the x-direction is $-K_x \partial c / \partial x$, so an equivalent velocity, the "turbulent flux velocity," can be defined such that

$$u_f c = -K_x \frac{\partial c}{\partial x} \quad \text{A-2}$$

or

$$u_f = - \frac{K_x}{c} \frac{\partial c}{\partial x} . \quad \text{A-3}$$

In a similar manner, in the other directions, the turbulent flux velocity will be

$$v_f = - \frac{K_y}{c} \frac{\partial c}{\partial y} \quad \text{A-4}$$

and

$$w_f = - \frac{K_z}{c} \frac{\partial c}{\partial z} . \quad \text{A-5}$$

If a tensor eddy diffusivity were used, the turbulent flux velocity could be written as

$$u_{fi} = - \sum_j \frac{K_{ij}}{c} \frac{\partial}{\partial x_j} , \quad \text{A-6}$$

where the subscripts are used for the three directions. This is the novel feature at the heart of the method - the diffusion terms are incorporated into a velocity. With these definitions, Eq. (A-1) becomes

$$\frac{\partial c}{\partial t} + \bar{u} \frac{\partial c}{\partial x} + \bar{v} \frac{\partial c}{\partial y} + \bar{w} \frac{\partial c}{\partial z} = - \frac{\partial}{\partial x} (u_f c) - \frac{\partial}{\partial y} (v_f c) - \frac{\partial}{\partial z} (w_f c) \quad \text{A-7}$$

or by substituting the divergence of the mean wind fluxes, ($\bar{u}c$, $\bar{v}c$ and $\bar{w}c$):

$$\begin{aligned} \frac{\partial c}{\partial t} + \frac{\partial (\bar{u}c)}{\partial x} + \frac{\partial (\bar{v}c)}{\partial y} + \frac{\partial (\bar{w}c)}{\partial z} - c \left(\frac{\partial \bar{u}}{\partial x} + \frac{\partial \bar{v}}{\partial y} + \frac{\partial \bar{w}}{\partial z} \right) = \\ - \frac{\partial (u_f c)}{\partial x} - \frac{\partial (v_f c)}{\partial y} - \frac{\partial (w_f c)}{\partial z} . \end{aligned} \quad \text{A-8}$$

We will now restrict our consideration to a divergence-free mean velocity (an incompressible mean flow) field which can be expressed as

$$\frac{\partial \bar{u}}{\partial x} + \frac{\partial \bar{v}}{\partial y} + \frac{\partial \bar{w}}{\partial z} = 0 . \quad \text{A-9}$$

That is, the mean velocity field ($\bar{u}, \bar{v}, \bar{w}$) is solenoidal. Thus, the term multiplying the concentration in Eq. A-8 is zero and

the remaining terms can be regrouped to give

$$\frac{\partial c}{\partial t} = - \frac{\partial (u+u_f)c}{\partial x} - \frac{\partial (v+v_f)c}{\partial y} - \frac{\partial (w+w_f)c}{\partial z} \quad . \quad \text{A-10}$$

It is apparent in this form of the diffusion equation that the concentration is being transported by the sum of the mean and turbulent flux velocities. This sum, called the "total equivalent transport velocity," is

$$u = \bar{u} + u_f \quad v = \bar{v} + v_f \quad w = \bar{w} + w_f \quad . \quad \text{A-11}$$

The diffusion equation then reduces to the form

$$\frac{\partial c}{\partial t} + \frac{\partial uc}{\partial x} + \frac{\partial vc}{\partial y} + \frac{\partial wc}{\partial z} = 0 \quad . \quad \text{A-12}$$

To complete the discussion, the boundary conditions for the original problem must be transformed into conditions within the field of fictitious total velocities. For the original problem governed by Eq. A-1, the boundary conditions will involve specification of the domain boundaries of the vector of total material flux, i.e., the vector F having components:

$$\begin{aligned} F_x &= \bar{u}c - K_x \frac{\partial c}{\partial x} \\ F_y &= \bar{v}c - K_y \frac{\partial c}{\partial y} \\ F_z &= \bar{w}c - K_z \frac{\partial c}{\partial z} \end{aligned} \quad \text{A-13}$$

Evidently,

$$F_x = uc \qquad F_y = vc \qquad F_z = wc \qquad A-14$$

so that the vector F is directly proportional to the fictitious total velocity vector. For typical boundary conditions the flux normal to a boundary is required to be zero (simulating an impervious surface).

The 3-D EXPLOR code uses the same wind field and diffusivity prescription as described above for 2-D EXPLOR, except that it is restricted to a constant flow as a function of height, unmodified by terrain. Special wind conditions, such as lee waves, building wakes, etc., must be specially input.

APPENDIX B

SAMPLE 3D CALCULATION

Since no real data have become available in which three dimensions are required, some results from a sample calculation are given. The road and terrain for a test case is shown in Figure B.1. The five rectangles represent five levels in the vertical direction. A double freeway is visible in the bottom layer. The wind is blowing from the upper left.

A problem was generated and allowed to run for several cycles, a number fewer than required for a steady state. At that point, a series of three machine generated contour plots was done, one perpendicular to each of the axes.

In Figure B.2 is shown the plot of the x - y plane for the bottom level. The numbers in the graph are relative values and should not be interpreted in an absolute sense. Notice that the higher concentrations (larger numbers) are found at the base of the hill, where they have been trapped.

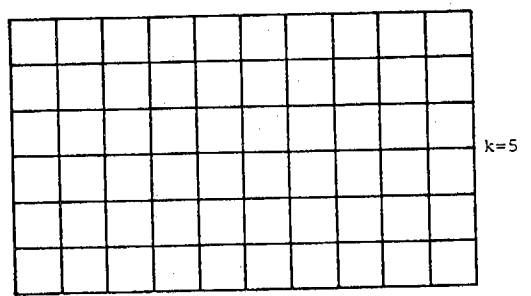
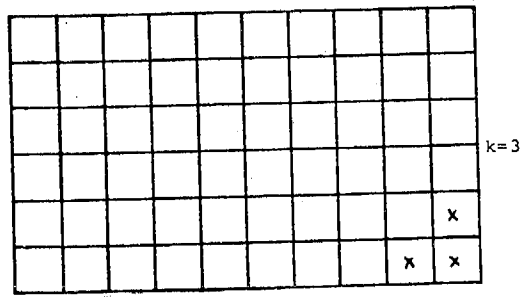
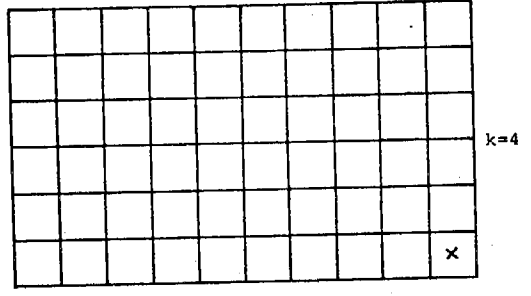
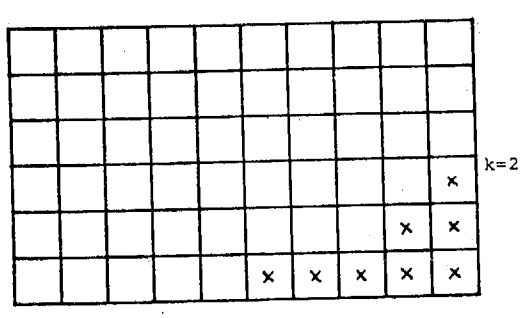
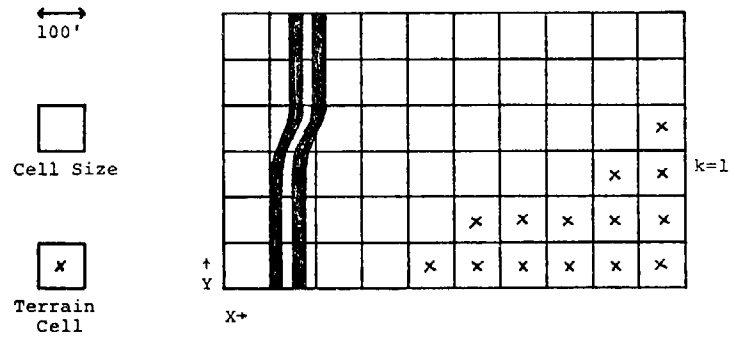


Figure B.1 Road and terrain locations in sample 3D EXPLOR calculation

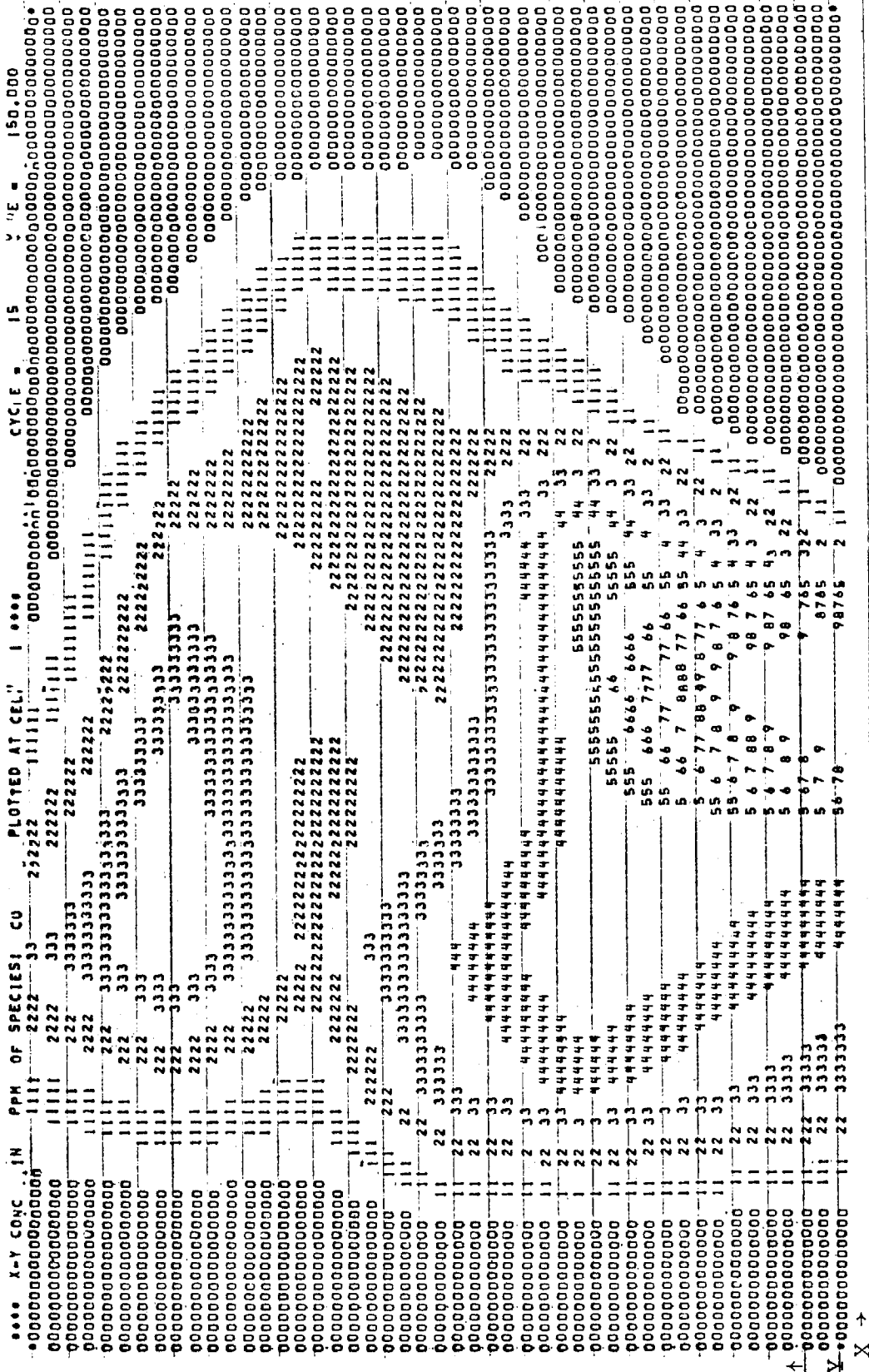


Figure B.2 Contour plot for CO in the X-Y plane for the bottom level

In Figure B-3 is shown the plot in the x - z plane for the third y cell. The pollutant has been trapped by the hill and is forcing its way over the top, as represented by the non-zero concentrations at the top of the graph.

Figure B-4 is the y - z plane plot along the third x cell, or just to the right of the freeway. Since the freeway bends, the right hand portion of the plot is closer to the source and has higher concentrations.

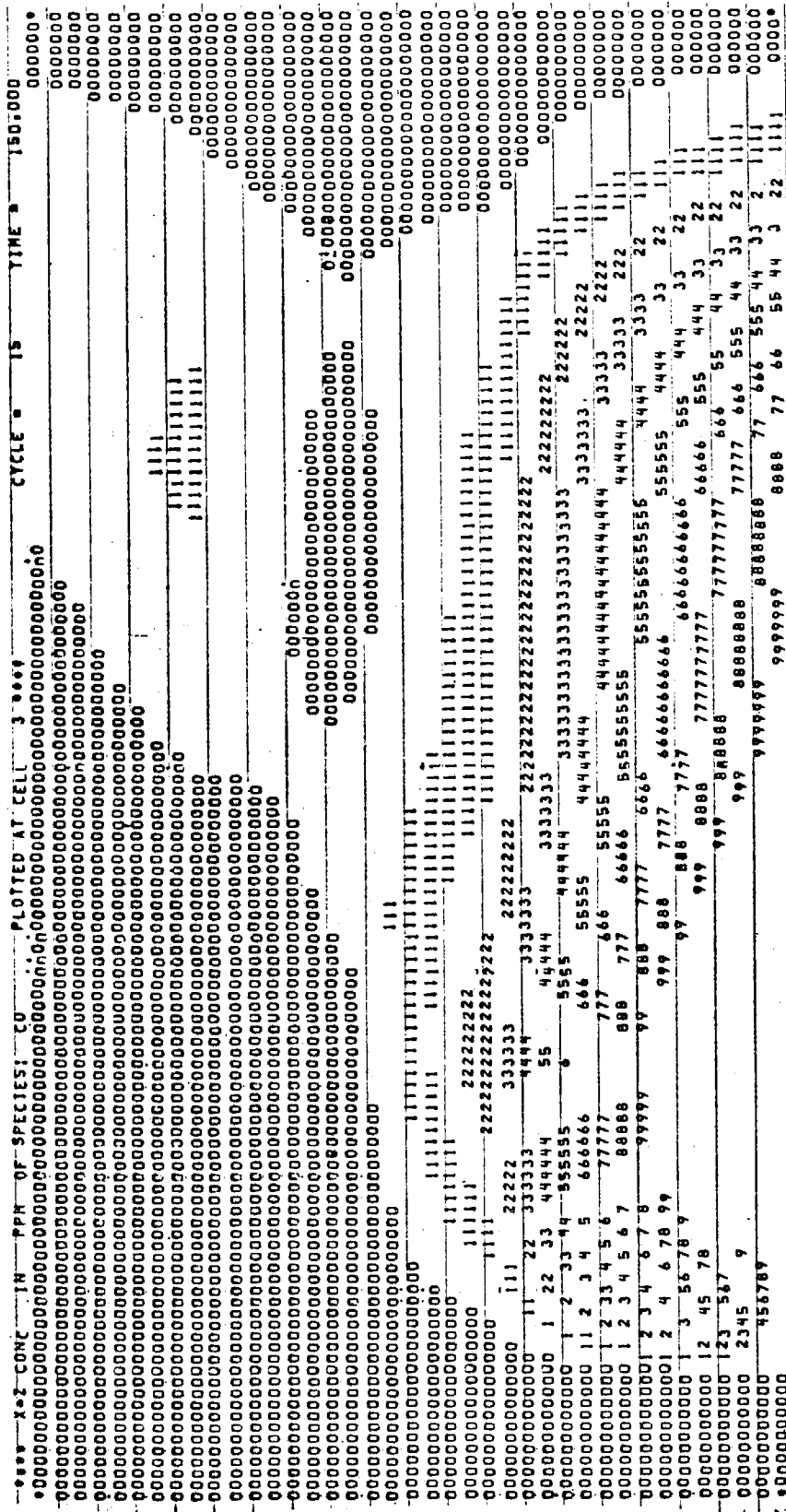


Figure B.3 Contour plot for CO in the X-Z plane at the third Y cell

